The Secular Evolution of a Close Ring–Satellite System: The Excitation of Spiral Bending Waves at a Nearby Gap Edge

Joseph M. Hahn

Space Science Institute
10500 Loring Drive
Austin, TX, 78750
email: jhahn@spacescience.org
phone: 512-291-2255

Accepted for publication in the *Astrophysical Journal*
April 30, 2007

ABSTRACT

The secular perturbations exerted by an inclined satellite orbiting in a gap in a broad planetary ring tends to excite the inclinations of the nearby ring particles, and the ring's self–gravity can allow that disturbance to propagate away in the form of a spiral bending wave. The amplitude of this spiral bending wave is determined, as well as the wavelength, which shrinks as the waves propagate outwards due to the effects of the central planet's oblateness. The excitation of these bending waves also damps the satellite's inclination I. This secular I damping is also compared to the inclination excitation that is due to the satellite's many other vertical resonances in the ring, and the condition for inclination damping is determined. The secular I damping is likely responsible for confining the orbits of Saturn's two known gap–embedded moons, Pan and Daphnis, to the ring plane.

Subject headings: planets: rings

1. Introduction

Secular gravitational perturbations can play a significant role in determining the global structure and the long–term evolution of a disk–companion system. A well–known example is the circumstellar dust disk at β Pictoris, whose broad but gentle warp is thought to be due to the secular gravitational perturbations exerted by an unseen planetary system

(Mouillet et al. 1997). Secular perturbations from an eccentric planet can also make a dust–disk appear lopsided, too (Wyatt et al. 1999). Secular perturbations are those forces that are due to the time–independent part of a companion's gravitational potential, and such perturbations are equivalent to the gravitational forces that arise when a perturber's mass is spread about its orbital ellipse (Murray & Dermott 1999). Consequently, the long–term secular evolution of a disk–companion system is conveniently modeled by treating it as a system of gravitating rings (Hahn 2003), an approach that will also be employed here.

When the perturber's orbit is eccentric or inclined, its secular perturbations can excite the orbital eccentricities or inclinations of the disk particles, as well as cause the orbits of the disk particles to precess over time. Large eccentricities e or inclinations I can also be excited at a secular resonance, which is a site where the disk matter precesses in sync with one of the eigenfrequencies that describe the perturber's precession. However, substantial e's and I's can also be excited elsewhere at non–resonant sites in the disk, with greater excitation occurring nearer the perturber. In fact, it is these non–resonant secular perturbations of the disk that are the focus of this study.

If the disk has internal forces, such as pressure or self–gravity, then those internal forces can also transmit the companion's disturbances across the disk. For instance, an inclined planet orbiting in a circumstellar gas disk can excite a global warp that is facilitated by the disk's internal pressure (Lubow & Ogilvie 2001). And if an eccentric companion inhabits a gap in the gas disk, its secular perturbations can launch a density wave at the gap edge having such a long wavelength that a global standing wave emerges (Goldreich & Sari 2003). But if the disk is instead gravity–dominated, then the companion can launch spiral density or spiral bending waves at its secular resonances in the disk (Ward & Hahn 1998, 2003). These phenomena are also relevant to studies of extra–solar planets, since any dissipation in the disk facilitates a transfer of angular momentum between the disk and the companion in a manner that tends to drive its eccentricity or inclination to zero.

The following will examine the secular evolution of a related system: of a small satellite that inhabits a narrow gap in a broad planetary ring, both of which are orbiting an oblate central planet. It will be shown below that an inclined satellite can launch a spiral bending wave that propagates outwards and away from the gap's outer edge. The amplitude and wavelength of this spiral bending wave is assessed below, as well as the rate at which this wave–action damps the satellite's inclination. This secular inclination–damping mechanism is then compared to the inclination excitation that is due to the satellite's many other vertical resonances in the ring (e.g., Borderies et al. 1984). We then quantify when this secular damping dominates over the resonant excitation, and show that this secular interaction is likely responsible for confining Saturn's two known gap–embedded moons, Pan and Daphnis,

to the ring plane.

2. Equations of motion

Begin by considering a planetary ring that is perturbed by a single satellite, with both orbiting an oblate planet. To assess the disturbance that the satellite might launch in this ring, the Lagrange planetary equations will be used; they give the rates at which a ring particle's orbital inclination I and longitude of ascending node Ω varies with time t:

$$\dot{I} \simeq -\frac{1}{na^2 I}\frac{\partial R}{\partial \Omega} \quad \text{and} \quad \dot{\Omega} \simeq \frac{1}{na^2 I}\frac{\partial R}{\partial I}, \tag{1}$$

where R is the disturbing function for a ring particle having a semimajor axis a and mean motion $n \simeq \sqrt{GM/a^3}$, where G is the gravitation constant and M is the mass of the central planet (Murray & Dermott 1999), and all inclinations are small, $I \ll 1$. The total disturbing function for a ring particle is $R = R_{disk} + R_{sat} + R_{obl}$, where the three terms account for the gravitational perturbations that are due to ring's gravity (which we treat here as a broad disk), the satellite's perturbations, and that due to the planet's oblate figure. The particle's equations of motion is thus the sum of three parts:

$$\dot{I} = \dot{I}\Big|_{disk} + \dot{I}\Big|_{sat} \quad \text{and} \quad \dot{\Omega} = \dot{\Omega}\Big|_{disk} + \dot{\Omega}\Big|_{sat} + \dot{\Omega}\Big|_{obl}, \tag{2}$$

noting that oblateness does not alter inclinations. And because we are only dealing with the system's secular perturbations, the semimajor axes of all bodies are constant (Brouwer & Clemence 1961).

The amplitude of a spiral bending wave that is in a steady–state does not vary with time, so the disk inclinations obey $\dot{I}(a) = 0$ throughout the disk. A persistent spiral pattern must also rotate with a constant angular velocity ω, so

$$\dot{I}\Big|_{disk} = -\dot{I}\Big|_{sat} \tag{3}$$

$$\text{and} \quad \omega = \dot{\Omega}\Big|_{disk} + \dot{\Omega}\Big|_{sat} + \dot{\Omega}\Big|_{obl} = \text{constant}. \tag{4}$$

The following subsection will use the first equation to solve for the wave amplitude $I(a)$ throughout the disk. The next subsection will then use the other equation to solve for the bending waves' dispersion relation $\omega(k)$, which in turn provides the wavenumber k of the spiral bending wave, and the wave's radial velocity.

2.1. wave amplitude

Begin by examining how the planetary ring perturbs itself. The ring is to be regarded as a broad disk that is composed of many narrow, concentric annuli. Each annulus has mass $\delta m(a)$, inclination $I(a)$, and longitude of ascending node $\Omega(a)$, all of which are to be regarded as functions of the rings' semimajor axes a. For the moment we will assume that all rings are circular, noting that we will deal with the system's eccentricity evolution in a followup study (Hahn 2007). Suppose that the annulus at a is perturbed by another annulus of mass $\delta m'$ and radius a'; the disturbing function for the perturbed annulus is

$$\delta R = -\frac{G\delta m'}{4a}\alpha\tilde{b}^{(1)}_{3/2}(\alpha)\left[\frac{1}{2}I^2 - II'\cos(\Omega-\Omega')\right], \tag{5}$$

where a, I, Ω are the orbit elements of the perturbed annulus, and the primed quantities refer to the perturbing annulus (Hahn 2003). The softened Laplace coefficient appearing in the above is

$$\tilde{b}^{(1)}_{3/2}(\alpha) = \frac{2}{\pi}\int_0^\pi \frac{\cos(\varphi)d\varphi}{[(1+\alpha^2)(1+\mathfrak{h}^2) - 2\alpha\cos\varphi]^{3/2}}, \tag{6}$$

and it is a function of the semimajor axis ratio $\alpha = a'/a$, where $\mathfrak{h} = h/a \ll 1$ is the disk's vertical scale height h in units of semimajor axis a. Note that when the disk is infinitesimally thin, $\mathfrak{h} = 0$, and the disturbing function δR is equivalent to that due to a point–mass $\delta m'$ (e.g., Brouwer & Clemence 1961).

It will be convenient to replace the ring mass $\delta m'$ with $2\pi\sigma' a' da'$, where $\sigma' = \sigma(a')$ is the mass surface density of the annulus of radius a' and radial width da'. We will also write its semimajor axis as $a' = a(1+x')$, where $x' = (a'-a)/a = \alpha - 1$ is the fractional distance between the perturbing ring a' and the perturbed ring a. For the moment we will consider a one-sided disk—one that orbits wholly exterior to the satellite, where Δ is the fractional distance between the satellite's orbit and the disk's inner edge; the geometry is sketched in Fig. 1. The disturbing function for ring a due to perturbations from ring a' can now be written as

$$\delta R = -\frac{1}{2}\mu'_d(na)^2\tilde{b}^{(1)}_{3/2}(x')\left[\frac{1}{2}I^2 - II'\cos(\Omega-\Omega')\right]dx' \tag{7}$$

where $\mu'_d \equiv \pi\sigma' a'^2/M$ is the ring's so–called normalized disk mass, $dx' = da'/a$ is the perturbing ring's fractional width, and $\tilde{b}^{(1)}_{3/2}(x')$ is shorthand for Eqn. (6) evaluated at $\alpha = 1 + x'$. Then according to Eqn. (1), ring a' will alter the inclination of ring a at the rate

$$\delta\dot{I} = -\frac{1}{na^2 I}\frac{\partial(\delta R)}{\partial\Omega} = \frac{1}{2}\mu'_d n\tilde{b}^{(1)}_{3/2}(x')I'\sin(\Omega-\Omega')dx'. \tag{8}$$

2.1.1. ring–disk evolution

The total rate at which the entire disk alters the inclination of ring a is the above with x' integrated across the disk, from $-x$ to $+\infty$ (see Fig. 1), so

$$\dot{I}\Big|_{disk} = \int_{disk} \delta\dot{I} = \frac{1}{2} n \int_{-x}^{\infty} \mu_d'(x') \tilde{b}_{3/2}^{(1)}(x') I'(x') \sin(\Omega - \Omega') dx'. \tag{9}$$

As one might expect, this integral is dominated by the contributions from nearby annuli that lie a small distance x' away. In the $|x'| \ll 1$ limit, the softened Laplace coefficient is

$$\tilde{b}_{3/2}^{(1)}(x') \simeq \frac{2}{\pi(x'^2 + 2\mathfrak{h}^2)} \tag{10}$$

(Hahn 2003). Because of the steep dependence of $\tilde{b}_{3/2}^{(1)}$ on x', we can replace the inclination $I'(x')$ and disk mass $\mu_d'(x')$ with their values evaluated at the perturbed ring at $x' = 0$, so $I' \simeq I$ and $\mu_d' \simeq \mu_d = \pi\sigma a^2/M$, and also pull them out of the integral so that

$$\dot{I}\Big|_{disk} \simeq \frac{\mu_d I n}{\pi} \int_{-x}^{\infty} \frac{\sin[\Omega - \Omega'(x')]}{x'^2 + 2\mathfrak{h}^2} dx'. \tag{11}$$

Most of the contributions to this integral will be due to nearby annuli that lie a wavelength $\lambda \simeq 2\pi/|k|$ away, where k is the wavenumber of the spiral bending wave.

A spiral wave has a wavenumber $k(a) = -\partial\Omega/\partial a$ (Eqn. A2), so the $\Omega - \Omega'$ in the above is

$$\Omega(a) - \Omega'(a') = -\int_{a'}^{a} k(r) dr. \tag{12}$$

In general, the wavenumber $k(a)$ will vary with semimajor axis a. However, considerable progress can be made if we assume that k is constant over a wavelength, so $\Omega - \Omega' \simeq -k(a - a') = kax'$. Then Eqn. (11) becomes

$$\dot{I}\Big|_{disk} \simeq \frac{1}{\pi} A_H(|k|ax) \mu_d I k a n \tag{13}$$

after replacing the x' integration variable with $y = |k|ax'$, and noting that Eqn. (11) is odd in y. In the above, the function $A(z)$ is a dimensionless measure of the warped disk's perturbation of itself:

$$A_H(z) \equiv \int_z^{\infty} \frac{\sin y}{y^2 + H^2} dy, \tag{14}$$

where $z = |k|ax$ is the distance from the ring–edge in units of 2π wavelengths, and the dimensionless wavenumber $H \equiv \sqrt{2}\mathfrak{h}|k|a$ is roughly the disk's vertical thickness in wavelength

units. The function $A_H(z)$ is also plotted in Fig. 2. We will be interested in a disk whose vertical thickness is small compared to the wavelength, so $H \ll 1$, and $A_H(z) \simeq \sin(z)/z - \mathrm{Ci}(z)$, where $\mathrm{Ci}(z)$ is the cosine integral of Abramowitz & Stegun (1972). Also keep in mind that these results assumed that the wavenumber k varies little over a single wavelength; subsection 2.2.2 will note when this approximation breaks down.

2.1.2. ring–satellite evolution

The ring at semimajor axis a is also being perturbed by the satellite, and that ring's disturbing function R_s due to the satellite is Eqn. (5) with $\delta m'$ replaced by the satellite's mass m_s:

$$R_s = -\frac{1}{4}\mu_s (na)^2 \alpha \tilde{b}^{(1)}_{3/2}(\alpha) \left[\frac{1}{2}I^2 - I I_s \cos(\Omega - \Omega_s)\right], \tag{15}$$

where $\mu_s = m_s/M$ is the satellite's mass in units of the central planet's mass, and $\alpha = a_s/a = (1 + \Delta + x)^{-1} \simeq 1 - (\Delta + x)$. The satellite's perturbation thus causes the ring's inclination to vary at the rate

$$\dot{I}\Big|_{sat} = -\frac{1}{na^2 I}\frac{\partial R_s}{\partial \Omega} = \frac{1}{4}\mu_s n \alpha \tilde{b}^{(1)}_{3/2}(\alpha) I_s \sin(\Omega - \Omega_s). \tag{16}$$

For a ring in the wave–excitation zone, *i.e.*, near the satellite,

$$\alpha \tilde{b}^{(1)}_{3/2}(\alpha) \simeq \frac{2}{\pi(x + \Delta)^2}, \tag{17}$$

since the ring lies a fractional distance $x + \Delta$ away from the satellite (see Fig. 1), with both presumably well separated such that $\Delta \gg \mathfrak{h}$. We also write the above longitude difference as $\Omega - \Omega_s \simeq -kax + \phi_o$, where the angle ϕ_o allows for the possibility that the annulus nearest the satellite at $x = 0$ may have a longitude of ascending node that differs from the satellite's node Ω_s by angle ϕ_o. Thus

$$\dot{I}\Big|_{sat} \simeq \frac{\mu_s I_s n}{2\pi(x + \Delta)^2} \sin(-kax + \phi_o) \tag{18}$$

is the rate at which the satellite alters a ring's inclination.

2.1.3. wave amplitude

When the wave is in steady–state, the two I–excitation rates, Eqns. (13) and (18), are balanced, which yields the amplitude of the bending wave:

$$\frac{I(z)}{I_s} = \frac{|k|a}{2}\frac{\mu_s}{\mu_d}\frac{\sin(z - s_k\phi_o)}{(z + |k|a\Delta)^2 A_H(z)} \tag{19}$$

where $s_k = \mathrm{sgn}(k)$ and $z = |k|ax$ is the downstream distance in units of 2π wavelengths. Far downstream, where $z \gg 1$, we expect $I(z) \to$ constant. For $z \gg 1$, $\mathrm{Ci}(z) \simeq \sin(z)/z - \cos(z)/z^2 + \mathcal{O}(z^{-3})$ (Abramowitz & Stegun 1972), so $A_H(z) \simeq \cos(z)/z^2$ downstream; see Fig. 2. So if $I(z)$ is to be a finite constant, then the longitude offset must be $\phi_o = \pm\pi/2$, and $I/I_s \simeq -(|k|a/2)(\mu_s/\mu_d)s_k \sin\phi_o$. Of course, these inclinations must also be positive, so $\sin\phi_o = \pm 1 = -s_k$, and the bending wave amplitude becomes

$$\frac{I}{I_s} \simeq \frac{|k_0|a\mu_s}{2\mu_d}, \tag{20}$$

where $|k_0|$ is the initial wavenumber at $x = 0$, where the wave is excited at the disk's inner edge. To make further use of this result, we still need the initial wavenumber k_0, which we get from the waves' dispersion relation.

2.2. dispersion relation

The waves' dispersion relation is obtained from Eqn. (4), with each term in that equation assessed below. The first term, $\dot{\Omega}\Big|_{disk}$, is the rate at which the disk drives its own precession. Again we calculate that rate by treating the disk as numerous narrow annuli. The rate that annulus a precesses due to the secular perturbations from the annulus at a' is

$$\delta\dot{\Omega} = \frac{1}{na^2 I}\frac{\partial(\delta R)}{\partial I} = -\frac{1}{2}\mu_d' n \tilde{b}_{3/2}^{(1)}(x') \left[1 - \frac{I'(x')}{I}\cos(\Omega - \Omega')\right] dx' \tag{21}$$

where δR is Eqn. (7). The total precession rate due to the disk's self–gravity is $\dot{\Omega}\Big|_{disk} = \int_{disk} \delta\dot{\Omega}$, where the integration proceeds across the entire disk. Again, the integrand is a steep function of x', due to the softened Laplace coefficient, Eqn. (10), which allows us to replace the quantities $I'(x')$ and $\mu_d'(x')$ with the constants I and μ_d. The disk's precession rate due to its self–gravity then becomes

$$\dot{\Omega}\Big|_{disk} \simeq -\frac{2}{\pi}\mu_d n \int_{-x}^{\infty} \frac{\sin^2(|k|ax'/2)}{x'^2 + 2\mathfrak{h}^2} dx' \tag{22}$$

$$= -B_H(|k|ax)|k|a\mu_d n \tag{23}$$

where

$$B_H(z) = \frac{2}{\pi}\int_{-z}^{\infty} \frac{\sin^2(y/2)}{y^2 + H^2} dy. \tag{24}$$

The function $B_H(z)$ is a dimensionless measure of the rate at which the disk drives its own precession. When the disk is much thinner than the wavelength, $H = \sqrt{2}\mathfrak{h}|k|a \ll 1$, and

$$B_H(z) \simeq \frac{1}{2} + \frac{1}{\pi}\mathrm{Si}(z) + \frac{\cos z - 1}{\pi z} \tag{25}$$

where $\mathrm{Si}(z)$ is the sine integral of Abramowitz & Stegun (1972). Far downstream, where $z \to \infty$, the B_H integral evaluates to

$$B_H^\infty \equiv \lim_{z\to\infty} B_H(z) = \frac{1}{H}(1 - e^{-H}). \tag{26}$$

Note that B_H^∞ is maximal when the dimensionless wavenumber is small, *i.e.*, $H \ll 1$, for which $B_H^\infty \simeq 1$. But if the disk is thick, $H \gg 1$ and $B_H^\infty \simeq H^{-1}$, which indicates that the disk's ability to sustain a bending wave is weakened when the disk is too thick.

Figure 2 also shows a numerical evaluation of $B_H(z)$ for a thin disk having $H = 0.01$. This Figure shows that $B_H(z)$ takes values of $1/2 \le B_H(z) \le 1$ for $z \ge 0$, with $B_H(0) = 1/2$ at the disk's inner edge, and that $B_H(z) \to 1$ downstream where $z \gg 1$, provided the disk is thin.

The satellite is also precessing the ring material orbiting nearest it; that precession occurs at the rate

$$\dot\Omega\Big|_{sat} = \frac{1}{na^2 I}\frac{\partial R_s}{\partial I} = -\frac{1}{4}\mu_s n\alpha \tilde b_{3/2}^{(1)}(\alpha)\left[1 - \frac{I_s}{I}\cos(\Omega - \Omega_s)\right] \tag{27}$$

$$\simeq -\left[\frac{\mu_s}{2\pi(x+\Delta)^2} + \frac{\mu_d \sin(|k|ax)}{\pi|k|a(x+\Delta)^2}\right] n \tag{28}$$

where I_s/I is replaced by the downstream wave amplitude, Eqn. (20). The first term is the familiar differential precession that would occur if the disk were massless. The second term, which is proportional to the disk mass μ_d, is the additional precession that is due to the torque that the satellite exerts upon the disk's spiral pattern.

The central planet's oblateness is also driving precession; the disturbing function for that perturbation is

$$R_{obl} \simeq -\frac{3}{4}J_2 I^2 \left(\frac{R_p}{a}\right)^2 (an)^2 \tag{29}$$

where J_2 is the planet's second zonal harmonic, and R_p is the planet's radius (Murray & Dermott 1999). Precession due to oblateness is then

$$\dot\Omega\Big|_{obl} = \frac{1}{na^2 I}\frac{\partial R_{obl}}{\partial I} = -\frac{3}{2}J_2\left(\frac{R_p}{a}\right)^2 n \tag{30}$$

$$\simeq \left[1 - \frac{7}{2}(x+\Delta)\right]\dot\Omega_s\Big|_{obl}, \tag{31}$$

where Eqn. (31) is a Taylor expansion of Eqn. (30) in the small quantity $x+\Delta$, and $\dot\Omega_s\Big|_{obl} \equiv -(3J_2/2)(R_p/a_s)^2 n_s$ is the rate at which the satellite's orbit precesses due to oblateness, where n_s is the satellite's mean motion.

Summing Eqns. (23), (28), and (31) provides the dispersion relation for the spiral bending waves:

$$\omega(|k|) \simeq -D(z)\mu_d|k|an - \frac{\mu_s n}{2\pi(x+\Delta)^2} + \left[1 - \frac{7}{2}(x+\Delta)\right] \dot{\Omega}_s\Big|_{obl}, \tag{32}$$

where

$$D(z) = B_H(z) + \frac{\sin z}{\pi(z+|k|a\Delta)^2}. \tag{33}$$

All terms in Eqn. (32) are negative, so the disk precesses in a retrograde sense. Note that if a spiral bending wave is to persist over time, then all parts of the disk must precess in concert. The dispersion relation, Eqn. (32), thus tells us how the wavenumber $|k(x)|$ must adjust throughout the disk in order for the spiral bending wave to precess coherently.

The first term in the dispersion relation is due to the disk's self–gravity. That term is proportional to $D(z)$, and it has two parts: self–precession that is driven by the bending wave itself (the B_H term D), and the additional precession that is driven by the satellite's torque on the spiral wave pattern [the latter term in Eqn. (33)]. The function $D(z)$ is plotted in Fig. 2, which shows that $1/2 \leq D(z) \leq 1$.

The second term in Eqn. (32) is the rate at which the satellite drives differential precession in the disk; this effect is most prominent nearest the satellite. The third term is the rate at which the oblate central planet drives differential precession, and this occurs all throughout the disk. Differential precession can inhibit wave–action by shredding the spiral pattern. But inspection of the dispersion relation suggests that bending waves can propagate, despite differential precession due to the satellite, when the satellite's mass is sufficiently small, *i.e.*, when $\mu_s \ll \mu_d|k|a\Delta^2$. The dispersion relation also tells us that the wavenumber $|k|$ must also increase with radial distance x in order to compensate for the additional differential precession that is due to the oblate central planet.

2.2.1. group velocity

The waves' group velocity is (Toomre 1969; Binney & Tremaine 1987)

$$c_g = \frac{\partial\omega}{\partial k} \simeq -s_k\mu_d an \tag{34}$$

upon setting $D(z) \simeq 1$ downstream; this is the rate at which the spiral bending wave propagates radially (Hahn 2003). Since the satellite is launching outward–propagating waves from the disk's inner edge, the group velocity must be positive, which implies that $s_k = \mathrm{sgn}(k) = -1$. Spiral waves having $k < 0$ are called *leading* waves. Note also that $\sin\phi_o =$

$-s_k = +1$, so $\phi_o = \pi/2$, which means that the longitude of ascending node at the disk's inner edge leads the satellite's node by 90°.

2.2.2. wavenumber k

The wavenumber k can be obtained by calculating the satellite's precession rate $\dot{\Omega}_s$. When the system is in steady–state, both the satellite and the spiral wave precess at the same rate, $\dot{\Omega}_s = \omega(|k|)$, which provides another equation for the wavenumber k.

The satellite's node Ω_s is being precessed by the disk and by the central planet, so

$$\dot{\Omega}_s = \dot{\Omega}_s\Big|_{disk} + \dot{\Omega}_s\Big|_{obl} \tag{35}$$

where $\dot{\Omega}_s\Big|_{disk} = \int_{disk} \delta\dot{\Omega}_s$ is the satellite's precession rate due to the entire disk, and where

$$\delta\dot{\Omega}_s = -\frac{1}{2}\mu'_d n_s \tilde{b}^{(1)}_{3/2}(\Delta + x') \left[1 - \frac{I'}{I_s}\cos(\Omega_s - \Omega')\right] dx' \tag{36}$$

is the satellite's precession rate due to a disk annulus of radius a' and mass $\delta m'$. This can be obtained from Eqn. (21) with n, a, I, Ω replaced by n_s, a_s, I_s, Ω_s and the separation $x' \to x' + \Delta$. The satellite's precession rate due to the entire disk is

$$\dot{\Omega}_s\Big|_{disk} = \int_{disk} \delta\dot{\Omega}_s \simeq -\frac{1}{\pi}\mu_d n_s \int_0^\infty (x' + \Delta)^{-2} \left[1 - \frac{I}{I_s}\cos(kax' - \phi_o)\right] dx' \tag{37a}$$

$$\simeq -\frac{\mu_d n_s}{\pi\Delta} - \frac{\mu_s n_s}{2\pi\Delta^2} S(|k_0|a\Delta) \tag{37b}$$

where

$$S(|k_0|a\Delta) \equiv |k_0 a\Delta|^2 \int_0^\infty \frac{\sin(y)dy}{(y + |k_0|a\Delta)^2}. \tag{38}$$

The first term in Eqn. (37b) is the rate at which the undisturbed disk precesses the satellite's orbit. The second term is the rate at which the bending wave, whose amplitude is proportional to μ_s by Eqn. (20), drives additional precession. The S function in that term is a dimensionless measure of the wave's contribution to the satellite's precession rate; that quantity depends on the wave's initial wavenumber $|k_0|$, and is plotted in Fig. 2, which shows that $0 \le S(|k_0|a\Delta) \le 1$.

Note that if the satellite instead orbited at the center of a narrow gap in the disk, then the first term in Eqn. (37b) would be doubled due to the disk matter orbiting interior to the satellite. We might also expect additional precession to occur due to any bending waves launched in this interior disk, but it will be shown below that this contribution is

unimportant. With this in mind, we will generalize Eqn. (37b) to account for a possible inner disk by writing

$$\dot{\Omega}_s\Big|_{disk} \simeq -\frac{\varepsilon\mu_d n_s}{\pi\Delta} - \frac{\mu_s n_s}{2\pi\Delta^2} S(|k_0|a\Delta) \tag{39}$$

where it is understood that $\varepsilon = 1$ if the disk is entirely exterior to the satellite, and that $\varepsilon = 2$ if the satellite instead orbits in the center of a gap whose fractional half–width is Δ. The satellite's total precession rate then becomes

$$\dot{\Omega}_s = \dot{\Omega}_s\Big|_{disk} + \dot{\Omega}_s\Big|_{obl} = -\frac{\varepsilon\mu_d n_s}{\pi\Delta} - \frac{\mu_s n_s}{2\pi\Delta^2} S(|k_0|a\Delta) + \dot{\Omega}_s\Big|_{obl}\,. \tag{40}$$

When the disk and satellite are in steady–state, the satellite and its spiral bending pattern precess in concert, so $\dot{\Omega}_s = \omega(|k|)$, which after some manipulation yields the dispersion relation

$$\pi D(z)|k|a\Delta = \varepsilon + \frac{\mu_c}{\mu_d}\left(1 + \frac{x}{\Delta}\right) + \frac{\mu_s}{2\mu_d\Delta} f(|k_0 a\Delta|, z), \tag{41}$$

where

$$f(|k_0 a\Delta|, z) = S(|k_0|a\Delta) - \frac{|k_0 a\Delta|^2}{(|k_0 a\Delta| + z)^2} \tag{42}$$

is another function of distance z and wavenumber $|k_0|$, one that is restricted to the interval $-1 \le f \le 1$, and

$$\mu_c \equiv \frac{21\pi}{4}\left(\frac{R_p\Delta}{a_s}\right)^2 J_2, \tag{43}$$

which will be called the critical disk mass.

2.2.3. limits on wave propagation

The disk's ability to sustain these bending waves is assessed by multiplying the dispersion relation (41) by $\sqrt{2}\mathfrak{h}/\pi\Delta$, which yields

$$HD = \frac{\sqrt{2}\mathfrak{h}}{\pi\Delta}\left[\varepsilon + \frac{\mu_c}{\mu_d}\left(1 + \frac{x}{\Delta}\right) + \frac{\mu_s f}{2\mu_d\Delta}\right] \tag{44}$$

where the dimensionless wavenumber $H = \sqrt{2}\mathfrak{h}|k|a$. Far downstream, where $z \gg 1$ and $D(z) = B_H^\infty = (1 - e^{-H})/H$ (see Eqns. 26 and 33), so $HD = 1 - e^{-H} < 1$. Wave propagation thus requires the right-hand side of Eqn. (44) to always be less than unity, which places an upper limit on the thickness of a disk that is able to sustain these bending waves, namely, that $\mathfrak{h} < \mathfrak{h}_{\max}$ where

$$\mathfrak{h}_{\max} \equiv \frac{\pi\Delta/\sqrt{2}}{\varepsilon + \mu_c/\mu_d + \mu_s/2\mu_d\Delta}, \tag{45}$$

upon setting $x = 0$ and $f = 1$ in order to obtain the most conservative limit on the disk's fractional thickness $\mathfrak{h}_{\rm max}$.

The remainder of this paper will assume that the disk is thin enough to sustain density waves, namely, that $\mathfrak{h} \ll \mathfrak{h}_{\rm max}$, or equivalently that $H \ll 1$, so that $D \sim \mathcal{O}(1)$. Also recall that Section 2.2 anticipated a wave solution to occur when the satellite's mass is small. Specifically, when $\mu_s \ll 2\varepsilon\mu_d\Delta$, the right-most terms in Eqns. (41) or (44) may be neglected, which then provides the wavenumber k as a simple function of distance x in the disk:

$$|k| \simeq \frac{1}{\pi \bar{D} a \Delta} \left[\varepsilon + \frac{\mu_c}{\mu_d} \left(1 + \frac{x}{\Delta} \right) \right] \tag{46}$$

where $D(z)$ has been replaced with its average value over the first wavelength, $\bar{D}$. And if the disk is sufficiently massive, namely, that $\mu_d \gtrsim 18\mu_c/\varepsilon$, then the initial wavenumber at $x = 0$ is $|k_0|a\Delta \simeq \varepsilon/\pi\bar{D} \simeq 0.37$, where $\varepsilon = 1$ and $\bar{D} \simeq 0.87$ according to Fig. 2. In that limit, the first wavelength is $\lambda_0 = 2\pi/|k_0| \simeq 2\pi^2 \bar{D}\Delta a \simeq 17\Delta \cdot a$. However shorter wavelengths will result when μ_d does not exceeds the above threshold.

Plugging Eqn. (46) evaluated at $x = 0$ into Eqn. (20) then yields the wave amplitude in terms of the system's physical parameters:

$$\frac{I(x)}{I_s} \simeq \frac{\mu_s(\varepsilon + \mu_c/\mu_d)}{2\pi \bar{D} \mu_d \Delta}. \tag{47}$$

2.2.4. inclination damping

The satellite launches a spiral bending wave via its secular gravitational perturbations of the ring. Those perturbations tilt the orbital plane of the nearby ring particles, and they in turn tilt the orbits of the more distant parts of the disk. Tilting an annulus in the disk also tips that ring's angular momentum vector, so the excitation of a bending waves transmits *in–plane* angular momentum from the satellite to the disk. Consequently, wave–excitation damps the satellite's inclination I_s, and that rate can be calculated using the Lagrange planetary equation for $\dot{I}_s$.

The rate $\delta\dot{I}_s$ at which a single annulus in the disk damps the satellite's inclination I_s is Eqn. (8), again with $n, a, I, \Omega \to n_s, a_s, I_s, \Omega_s$ and $x' \to x' + \Delta$. Integrating the contributions by all annuli in the disk gives the satellite's total inclination–damping rate,

$$\dot{I}_s = \int_{disk} \delta\dot{I}_s = \frac{\mu_d I n_s}{\pi k_0 a \Delta^2} C(|k_0|a\Delta) \tag{48}$$

where k_0 is the initial wavenumber at the disk's inner edge, and the function

$$C(z) = z^2 \int_0^\infty \frac{\cos(y)dy}{(y+z)^2} = z + z^2 \left\{ \left[\mathrm{Si}(z) - \frac{\pi}{2} \right] \cos z - \mathrm{Ci}(z) \sin z \right\} \tag{49}$$

is shown in Fig. 3. Inserting Eqn. (20) into (48) and noting that $k_0 = -|k_0|$ then provides the inclination–damping rate in terms of the system's physical parameters:

$$\frac{\dot{I}_s}{I_s} = -\frac{C(|k_0|a\Delta)}{2\pi} \frac{\mu_s}{\Delta^2} n_s. \tag{50}$$

The reciprocal of the above gives the e–fold timescale for the satellite's inclination decay:

$$\tau_i = \frac{\Delta^2 P_{orb}}{C(|k_0|a\Delta)\mu_s}, \tag{51}$$

where $P_{orb} = 2\pi/n_s$ is the satellite's orbit period. Note that for a planet that is not too oblate (e.g., Section 2.2.2) $|k_0|a\Delta = 0.37$, so $C(|k_0|a\Delta) \simeq 0.24$ (Fig. 3). This inclination–damping rate is also confirmed below, in a numerical simulation of spiral bending waves launched in a planetary ring.

3. Simulations of spiral bending waves

The rings model of Hahn (2003) will be used to confirm the preceding results. The rings model treats the system as a set of N discrete gravitating annuli having semimajor axes a_j, inclinations I_j, nodes Ω_j, and half–thicknesses h_j. The model only considers the system's secular gravitational perturbations, so it also solves the same equations of motion, Eqns. (2), but the model does so without making any of the wave–assumptions invoked in Section 2.1. The model thus provides an independent check of the analytic results obtained above.

3.1. waves in an exterior disk

The rings model is used to simulate the spiral bending waves that are launched by an inclined satellite that orbits just interior to a disk. Figure 4 shows the amplitude of this bending wave as it advances across a disk. The system's parameters are detailed in Fig. 4. Those parameters do not correspond to any real ring–satellite system; rather, these parameters were chosen to illustrate the results of Section 2 in the limit in which those results were obtained, namely, that the satellite's mass is small, *i.e.*, $\mu_s \ll 2\mu_d\Delta$ so that Eqn. (46) is valid. Those parameters were also chosen so that the factor μ_c/μ_d appearing

in the wavenumber Eqn. (46) is 0.2, which causes the wavelength to slowly decrease with distance x as they propagate away. Nonetheless, the simulation reported in Fig. 4 does correspond loosely to a small ~ 10 km satellite orbiting just interior to ring whose surface density is similar to Saturn's main A ring.

Inspecting this system's angular momentum provides a quick check on the quality of this calculation. This system should conserve the in–plane component of its total angular momentum, $L_i = \frac{1}{2}\sum m_j n_j a_j^2 I_j^2$, where the sum runs over all rings and satellites in the system (Hahn 2003). The single–precision calculation shown in Fig. 4 conserves L_i with a fractional error of $|\Delta L_i/L_i| < 2 \times 10^{-5}$.

Note that the time for these waves to propagate a fractional radial distance $x = \Delta r/a$ is

$$t_{prop} = \frac{\Delta r}{c_g} = \frac{x P_{orb}}{2\pi\mu_d}, \tag{52}$$

where c_g is the waves' group velocity, Eqn. (34). The simulated disk has a normalized mass of $\mu_d = 5 \times 10^{-8}$ and a fractional width $x = 0.02$, so the anticipated propagation time is $t_{prop} = 64 \times 10^3$ orbits, which compares favorably with the simulation (see Fig. 4).

If the disturbance seen in Fig. 4 is indeed a spiral bending wave, then the disk's longitude of ascending node $\Omega(a)$ should steadily advance as a increases across the disk. This is confirmed in Fig. 5, which shows the waves' longitudes relative to the satellite's, $\Omega(a) - \Omega_s$. These are also the longitudes where the warped disk passes through the central planet's equatorial plane. Note that this disk will have its maximum elevation at longitudes 90° ahead of that seen in Fig. 5, with its minimum elevation at longitudes 90° behind. Note also that the longitude of the disk's inner edge is 90° ahead of the satellite's longitude, as expected. And since the wavenumber $k = -\partial\Omega/\partial a$ is negative, this spiral pattern is indeed a leading wave. We also note that once the bending wave is established in the disk, the disk's longitudes precess at the same rate as the satellite's, *i.e.*, $\dot{\Omega}(a) = \dot{\Omega}_s$, and that the disk's inclinations are constant, $\dot{I}(a) = 0$, which justifies our steady–state assumptions, Eqn. (3).

Figure 5 also plots the dimensionless wavenumber $|k|a\Delta$ across the disk at time $t = 75 \times 10^3$. This is the moment when the bending wave is just starting to reflect at the disk's outer edge, which accounts for the curve's raggedness there. Also plotted is the expected wavenumber, Eqn. (46), which compares favorably.

The rate at which the disk damps the simulated satellite's inclination I_s is shown in Fig. 6, where it is compared to the expected rate, Eqn. (50). That rate is calculated by noting that the waves' initial wavenumber is $|k_0|a\Delta \simeq 0.63$ at the disk's inner edge (see Fig. 5), so the C that appears in Eqn. (50) is $C(|k_0|a\Delta) = 0.32$, according to Fig. 3. The expected and observed inclination damping rates are in good agreement.

3.2. Satellite in a gap

The simulation described by Figs. 4 and 5 is a bit of fiction, since there are no known satellites orbiting just interior to a broad planetary ring. For instance, all of the major Saturnian satellites orbit exterior to Saturn's main rings. However there are two noteworthy exceptions: the small satellite Pan, which orbits in the Encke gap in Saturn's A ring, and Daphnis, which inhabits the Keeler gap in Saturn's A ring (Porco 2005).

A simulation of an inclined Pan as it orbits in the Encke gap is reported in Figure 7, which shows the state of this system at time $t = 7.5 \times 10^4$ orbits. This is the time required for Pan to launch a leading spiral bending wave at the gap's outer edge that then propagates to the simulated ring–system's outer edge. Figure 7 shows that waves' initial wavelength is $\lambda_0 = 0.0037 a_s \simeq 500$ km, and that their wavelength shrinks with distance x as they propagate towards the outer edge of the A ring, which lies a fractional distance $x = 0.024$ away. So if these waves are not otherwise damped en route by collisions among ring particles, their wavenumber will have grown to $|k|a \simeq 1.1 \times 10^4$ when they reach the A ring's outer edge (see Eqn. 46), which corresponds to wavelength of $\lambda = 2\pi/|k| \simeq 80$ km.

Figure 8 also shows the system at the later time $t = 1.5 \times 10^5$ orbits, which is when the wave has since reflect at the simulated ring's outer edge and returned to the launch site. Here we see the superposition of an outbound leading wave with an inbound trailing wave, which results in a standing bending wave throughout the disk. As the Figure shows, when the standing wave emerges, it arranges the disk's longitudes Ω such that they alternate between $-90°$ and $+90°$ of the satellite's node Ω_s at every half–wavelength. So if the waves launched by an inclined Pan do not get damped downstream, that bending wave will reflect at the outer A ring and return to Pan's vicinity where it can communicate its in–plane angular momentum back to the satellite. At this moment, inclination–damping then ceases.

Figures 7 and 8 also show that Pan does not launch any inward–propagating waves. Although the satellite's secular perturbations do excite inclinations at the gap's inner edge, those disturbances do not travel further inwards. The wavenumber $|k|$ for any disturbance

that might propagate in the interior disk is[1]

$$|k| \simeq \frac{1}{\pi \bar{D} a |\Delta|} \left[\varepsilon - \frac{\mu_c}{\mu_d} \left(1 + \left| \frac{x}{\Delta} \right| \right) \right], \tag{53}$$

which is identical to Eqn. (46) except for the sign on the disk mass term. Since the right hand side must be positive, Eqn. (53) tells us that waves in the inner disk can only propagate in the zone where $|x| < x_{in}$, where

$$x_{in} \equiv \left(\frac{\varepsilon \mu_d}{\mu_c} - 1 \right) |\Delta| \tag{54}$$

is the distance of the waves' maximum excursion inwards of the satellite's orbit. Getting waves to propagate inwards a significant distance thus requires the disk mass to be sufficiently high, namely, $\mu_d \gg \mu_c/2$, where $\varepsilon = 2$ for a gap–embedded satellite. Saturn's A ring has a disk mass of $\mu_d \sim 5 \times 10^{-8}$ and a critical disk mass of $\mu_c = 7.8 \times 10^{-8}$ (from Fig. 7 caption), so $\mu_d \gg \mu_c/2$ is not well–satisfied, and inward–propagating bending waves are precluded.

Also note that this simulation does not satisfy $\mu_d \gtrsim 18\mu_c/\varepsilon$, which means that the wavenumber k does varies substantially across that first wavelength (see Eqn. 46). A wavenumber that is nearly constant over that first wavelength is of course a key assumption of Sections 2–3, so the analytic results obtained there might seem not apply to Pan. Nonetheless, when those formulas are compared to the model results, we find that Eqn. (46) to be in excellent agreement with the wavenumber $k(x)$ exhibited by the simulated wave. But Eqn. (47) does overestimate the amplitude of this simulated wave by a factor of ~ 4, which in turn causes Eqn. (50) to overestimate Pan's inclination–damping rate by the same factor.

However Daphnis inhabits the narrower Keeler gap, whose fractional half width $\Delta = 1.1 \times 10^{-4}$ is a tenth that of the nearby Encke gap, so its μ_c is 100 times smaller, and $x_{in} \simeq 120|\Delta| = 0.013$, which corresponds to a physical distance of $x_{in} a_s \simeq 1800$ km, or about 10 wavelengths. So when the rings model is used to simulate the spiral waves that an inclined Daphnis would launch, we do indeed see a wave launched from the gap's inner edge.

---

[1]This wavenumber is obtained by repeating the derivation of Section 2 by applying that to an annulus in the inner disk whose semimajor axis is again $a = a_s(1 + x + \Delta)$, but with the distances x and Δ now understood as having negative values. So when integrating the net perturbation that the entire disk exerts on an annulus, the integration variable x' in Eqns. (9) and (22) now runs over $-\infty \leq x' \leq -x$. The net effect of this is to merely change the sign on certain terms: $\dot{I}_{disk}$ is $-1\times$Eqn (13), and $s_k = \mathrm{sgn}(k) = \sin\phi_i = +1$, where $\phi_i = \pi/2$ is the longitude offset between the inner gap edge and the satellite. Any inward–propagating waves in the inner disk are trailing, since $k > 0$. The argument of the sinusoid in Eqn. (28) also changes sign. Accounting for these sign changes then yields Eqn. (53).

That wave propagates inwards approximately a distance x_{in}, where it reflects and propagates outwards and across the Keeler gap. That satellite's simulated I–damping timescale is also in good agreement with the prediction, Eqn. (51).

4. External Vertical Resonances

A satellite orbiting near a planetary ring also excites inclinations at its many external vertical resonances in the ring. This also communicates in–plane angular momentum between the satellite and the ring, but in a manner that *excites* the satellite's inclination I_s. Borderies et al. (1984) calculate the rate at which the external resonances in a narrow ring of mass $\delta m'$ excite the satellite's inclination:

$$\delta \dot{I}_s = g \mu_s n_s |x'|^{-5} \frac{\delta m'}{M} I_s \tag{55}$$

where $g = 0.0118$, and x' is the satellite's fractional distance from the ring of mass $\delta m' = 2\pi\sigma a^2 dx'$. The satellite's total I–excitation rate is the above integrated across the entire disk, $\dot{I}_s = \int_{disk} \delta \dot{I}_s$. If the satellite orbits in the center of a gap in a broad planetary ring, the total excitation rate due to external vertical resonances is

$$\frac{\dot{I}_s}{I_s} = \frac{g \mu_s \mu_d n_s}{\Delta^4} \tag{56}$$

(Ward & Hahn 2003). So if the satellite's orbit is to remain confined to the ring plane, this I–excitation due to the satellite's external resonances must be smaller than the I–damping that results from its secular interaction with the ring, Eqn. (50). Comparing these two rates shows that the satellite's inclination is stable, *i.e.*, $\dot{I}_s < 0$, when its gap is sufficiently large, namely, when

$$\Delta^2 > \frac{2\pi g \mu_d}{C(|k_0| a \Delta)}. \tag{57}$$

Bending waves launched by Pan and Daphnis have initial wavenumbers of $|k_0| a \Delta \simeq 1$ (see Eqn. 46), so $C(|k_0| a \Delta) \simeq 0.3$ (see Fig. 3), and the requirement for inclination damping becomes $\Delta \gtrsim 0.5\sqrt{\mu_d}$. These satellites inhabit Saturn's A ring, which has a normalized disk mass of $\mu_d \simeq 5 \times 10^{-8}$, so their inclinations are stable if their gap half–widths are wider than $\Delta \gtrsim 1.1 \times 10^{-4}$. Pan easily satisfies this requirement ($\Delta = 0.0012$), while Daphnis marginally so ($\Delta = 1.1 \times 10^{-4}$). The I–damping timescale for Pan is quite short, only $\tau_i \simeq 1.7 \times 10^6$ orbits (e.g., four times Eqn. 51), which corresponds to $\tau_i \simeq 2700$ years. A comparable I–damping timescale is also obtained for Daphnis, whose size is about four times smaller than Pan's (Spitale et al. 2006), and whose gap is ten times narrower.

5. Summary and Conclusions

The secular perturbations exerted by an inclined satellite orbiting in a gap in a broad planetary ring tends to excite the inclinations of the nearby ring particles. The ring's self gravity then allows that disturbance to radiate away in the form of a spiral bending wave. The wavelength $\lambda = 2\pi/|k|$ of any outbound waves is obtained from Eqn. (46), which shows that λ decreases with distance x from the nearby gap edge. These wavelength variations are due to a competition between the disk's self gravity and the differential precession that is due to the oblate central planet. As an example, we find that an inclined Pan, which inhabits the Encke gap in Saturn's main A ring, would excite a bending wave having an initial wavelength of about 500 km. And if that wave manages to propagate out to the outer edge of the A ring without damping, the wavelength will then have shrunk down to about 80 km there.

A gap–embedded satellite will also try to launch a wave at the gap's inner edge, but the range of these waves is limited by how far they can propagate until their wavenumber has shrunk to zero; see Eqn. (53). That distance is controlled by the width of the gap, with a narrower gap resulting in a greater inward excursion; see Eqns. (54) and (43). For instance, Pan is unable to launch an inward–propagating wave, while Daphnis, which inhabits the narrower Keeler gap, could launch a disturbance that propagates inwards about 1% of its orbit before reflecting and propagating back out and across the Keeler gap.

The amplitude of this wave is given by Eqn. (47), and the excitation of this wave also damps the satellite's inclination quite vigorously, at a rate given by Eqn. (50). This I–damping mechanism also competes with the satellite's many other vertical resonances in the ring, which try to pump up the satellite's inclination (Borderies et al. 1984). However the secular I–damping will dominate when the satellite's gap is sufficiently wide, namely, when Eqn. (57) is satisfied. Saturn's gap–embedded moon Pan satisfies this requirement, while Daphnis is at the threshold. This secular phenomenon also damps inclinations on a very short timescale τ_i, which for these satellites is of order 3000 yrs (Eqn. 51). This of course assumes that these waves damp somewhere downstream, rather than reflecting at the ring's outer edge and returning to the launch site. But if these waves reflect and return without suffering significant damping, then a standing wave will emerge in the disk. That standing wave would also communicate some of its in–plane angular momentum back into the satellite's orbit, so further inclination–damping would cease. But if these waves instead damp downstream, then this secular phenomenon represents an important stabilizing influence that tends to confine a satellite's orbit to the ring plane. But this inclination–damping also shuts off any subsequent wave generation, so is seems unlikely that these waves might ever be observed in a planetary ring.

Finally, we note that the rings model employed here played a important role in guiding the analytic results obtained above. The model itself is a fairly easy–to–use set of IDL scripts, and other applications of this code are possible. For instance, the rings model has revealed that an eccentric satellite's secular perturbations can launch spiral density waves in a nearby ring, and the eccentricity damping that is associated with that phenomena will be assessed in a followup study (Hahn 2007). A copy of the rings model algorithm will also be made available to others upon request.

Acknowledgments

This research was initiated while the author was in residence at Saint Mary's University, and that portion of this research was supported by a Discovery Grant from the Natural Sciences and Engineering Research Council of Canada (NSERC). This work was also supported by a grant from NASA's Outer Planets Research Program. The author also thanks Jayme Derrah for composing Figure 1.

A. Appendix A

The disk's vertical displacement is $z(a, \theta, t) = a \sin I \sin(\theta - \Omega)$, where (a, θ) are the radial and azimuthal coordinates in the disk, and the inclination I and ascending node Ω should be regarded as functions of distance a and time t. When a spiral bending wave is present in the disk, the longitudes have the form

$$\Omega(a, t) = \Omega(a_0, 0) - \int_{a_0}^{a} k(r) dr + \omega t, \tag{A1}$$

where $\Omega(a_0, 0)$ is the longitude of the ascending node at some reference distance a_0 at time $t = 0$, $k(a)$ is the wavenumber of the spiral bending wave, and ω is the angular rate at which the spiral pattern rotates, also known as the pattern speed. The signs in the above expression are chosen to follow the convention that a $k < 0$ spiral is a *leading* spiral, which means that a curve having a constant $z(a, \theta)$ in the disk traces a spiral that advances in θ as a increases. Thus the wavenumber k can be written as

$$k = -\frac{\partial \Omega}{\partial a}, \tag{A2}$$

and the group velocity is

$$c_g = \frac{\partial \omega}{\partial k} \tag{A3}$$

(Toomre 1969; Binney & Tremaine 1987).

REFERENCES

Abramowitz, M. & Stegun, I. A. 1972, Handbook of Mathematical Functions (Handbook of Mathematical Functions, New York: Dover, 1972)

Binney, J. & Tremaine, S. 1987, Galactic dynamics (Princeton, NJ, Princeton University Press, 1987, 747 p.)

Borderies, N., Goldreich, P., & Tremaine, S. 1984, ApJ, 284, 429

Brouwer, D. & Clemence, G. M. 1961, Methods of celestial mechanics (New York: Academic Press, 1961)

Burns, J. A., Hedman, M. M., Tiscareno, M. S., Nicholson, P. D., Streetman, B. J., Colwell, J. E., Showalter, M. R., Murray, C. D., Cuzzi, J. N., Porco, C. C., & Cassini ISS Team. 2005, AAS/Division for Planetary Sciences Meeting Abstracts, 37,

Goldreich, P. & Sari, R. 2003, ApJ, 585, 1024

Hahn, J. M. 2003, ApJ, 595, 531

—. 2007, in preparation

Lubow, S. H. & Ogilvie, G. I. 2001, ApJ, 560, 997

Mouillet, D., Larwood, J. D., Papaloizou, J. C. B., & Lagrange, A. M. 1997, MNRAS, 292, 896

Murray, C. D. & Dermott, S. F. 1999, Solar system dynamics (Cambridge University Press)

Porco, C. C. 2005, IAU Circ., 8524, 1

Rosen, P. A., Tyler, G. L., Marouf, E. A., & Lissauer, J. J. 1991, Icarus, 93, 25

Spitale, J. N., Jacobson, R. A., Porco, C. C., & Owen, Jr., W. M. 2006, AJ, 132, 692

Toomre, A. 1969, ApJ, 158, 899

Ward, W. R. & Hahn, J. M. 1998, AJ, 116, 489

—. 2003, AJ, 125, 3389

Wyatt, M. C., Dermott, S. F., Telesco, C. M., Fisher, R. S., Grogan, K., Holmes, E. K., & Piña, R. K. 1999, ApJ, 527, 918

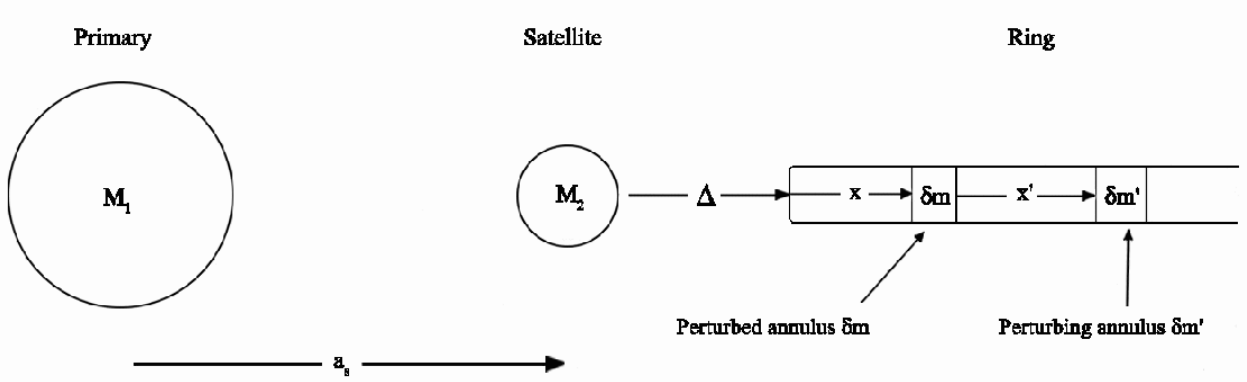

Fig. 1.— A schematic showing the geometry of the ring–satellite system, seen edge-on. A satellite of mass m_s and semimajor axis a_s orbits interior to a broad planetary ring that extends to infinity. The satellite's distance from the ring's inner edge is Δ in units of the satellite's semimajor axis a_s. A perturbed annulus in the ring has mass δm, and it lies a fractional distance x away from the ring's inner edge, while the perturbing ring has mass $\delta m'$ and lies a fractional distance x' from the perturbed ring.

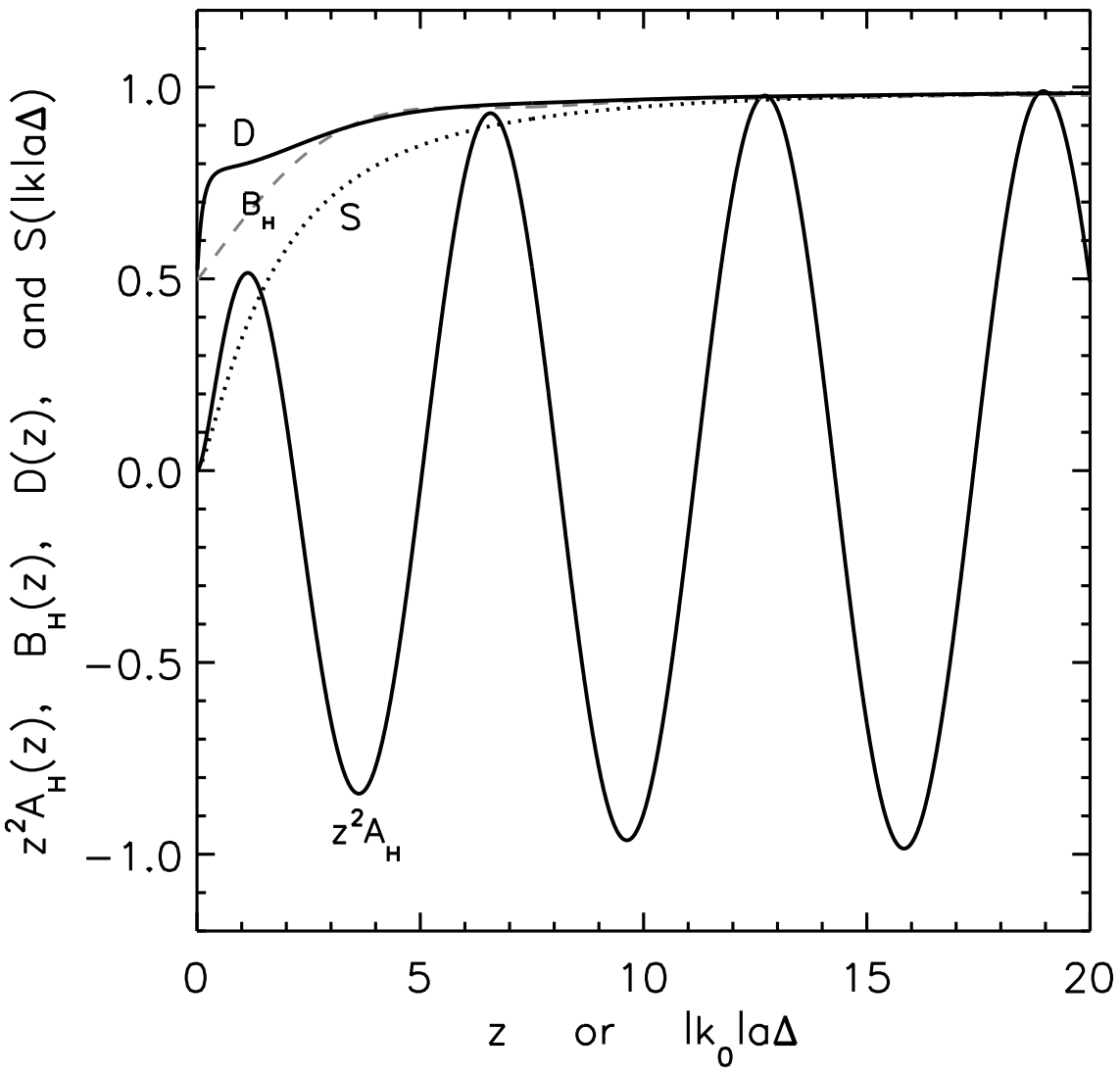

Fig. 2.— The functions $z^2 A_H(z)$ [from Eqn. (14), solid curve], $B_H(z)$ [Eqn. (24), dashed curve], $D(z)$ [Eqn. (33), solid curve], and $S(|k_0|a\Delta)$ [Eqn. (38), dotted] are evaluated numerically for a thin disk having $H = 0.01$. These curves are plotted versus $z = |k|ax$, which is the dimensionless distance from the ring's inner edge in units of 2π wavelengths, or versus the dimensionless wavenumber $|k_0|a\Delta$. The $D(z)$ function is evaluated with $|k|a\Delta = 0.37$, a value that is justified in Section 2.2.2. The average of $D(z)$ over the first wavelength, $0 \leq z \leq 2\pi$, is $\bar{D} \simeq 0.87$. Note also that $z^2 A_H(z) \simeq \cos z$ after the first wavelength.

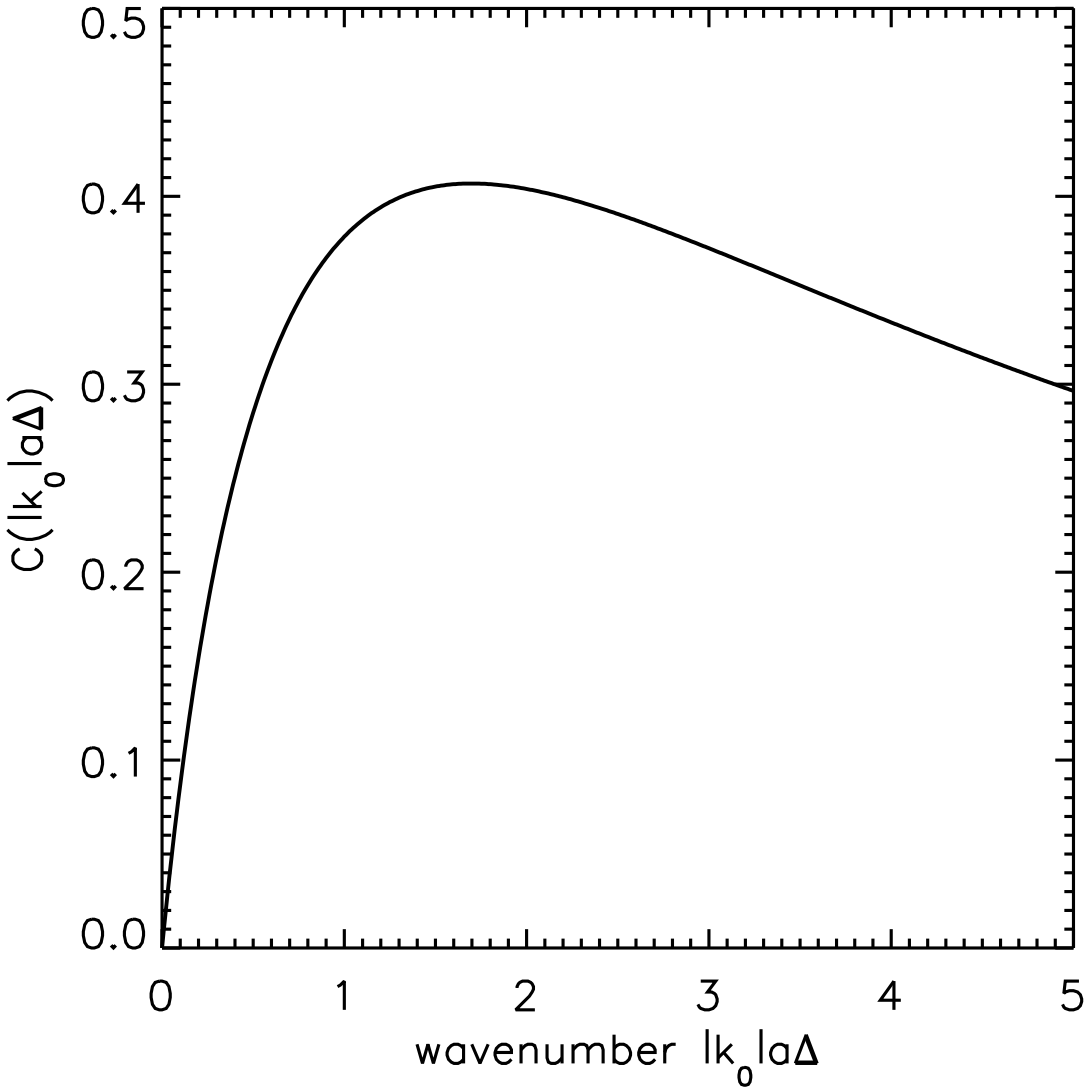

Fig. 3.— The function $C(|k_0|a\Delta)$ from Eqn. (49), plotted versus the dimensionless wavenumber $|k_0|a\Delta$.

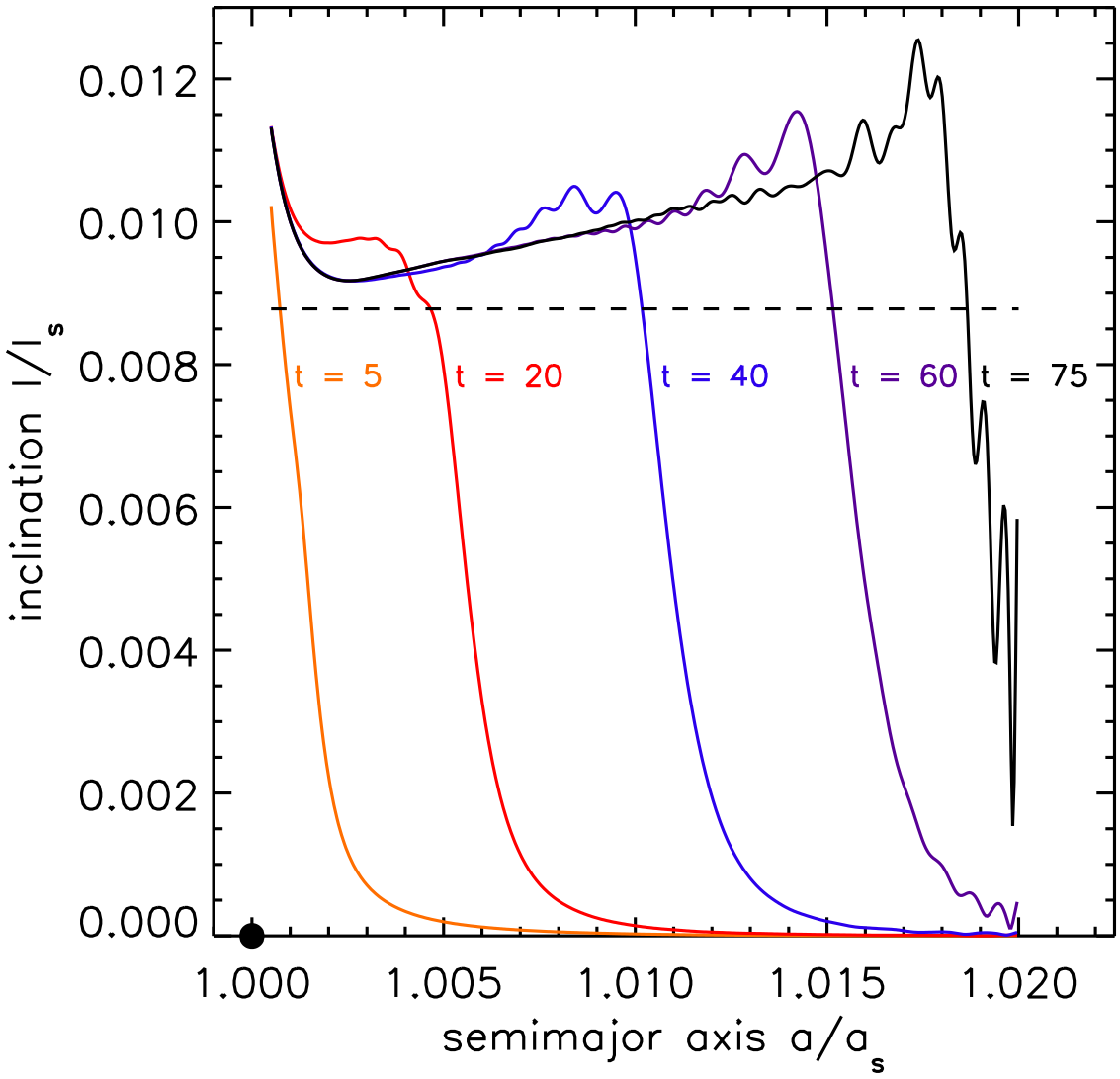
0.012
0.010
0.008
0.006
0.004
0.002
0.000
inclination I/I_s
t = 5
t = 20
t = 40
t = 60
t = 75
1.000
1.005
1.010
1.015
1.020
semimajor axis a/a_s

Fig. 4.— The rings model is used to simulate bending waves launched by an inclined satellite that orbits just interior to a disk. The satellite's normalized mass is $\mu_s = 10^{-12}$, and the disk is comprised of $N = 500$ rings having semimajor axes distributed over $1 + \Delta \leq a_j/a_s \leq 1.02$, where $\Delta = 5 \times 10^{-4}$ is the fractional distance between the satellite and the innermost ring. The rings' fractional masses are $\mu_r = 3.9 \times 10^{-12}$, so the normalized disk mass is $\mu_d = \pi\sigma r^2/M = \mu_r/2(\delta/a_s) = 5 \times 10^{-8}$, where the rings' fractional separations are $\delta/a_s = 0.02/N = 4 \times 10^{-5}$. The rings' fractional half–widths $\mathfrak{h}$ is also set equal to their separations δ/a_s. The central planet's zonal harmonic is $J_2 = 0.012$ and the planet's radius is $R_p/a_s = 0.45$, so the system's critical disk mass is $\mu_c = 1.0 \times 10^{-8}$ and $\mu_c/\mu_d = 0.2$. The satellite's initial inclination is $\sin I_s = 10^{-5}$, with all other rings initially having zero inclinations. The curves show the fractional amplitude of the bending wave, $I(a)/I_s$, as it advances across the disk, shown at selected times t in units of 10^3 orbital periods. The dashed line is the expected wave amplitude, Eqn. (47), with $\varepsilon = 1$.

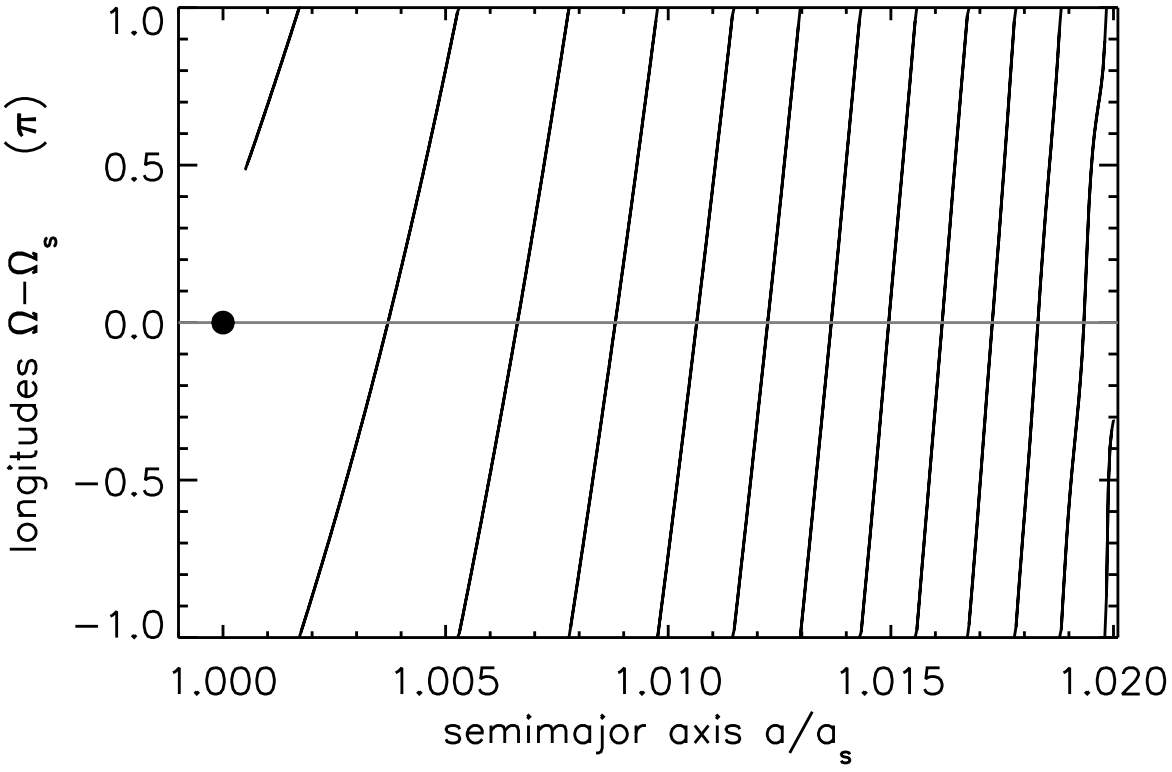
1.0
0.5
0.0
−0.5
−1.0
longitudes Ω−Ω_s (π)
1.000
1.005
1.010
1.015
1.020
semimajor axis a/a_s

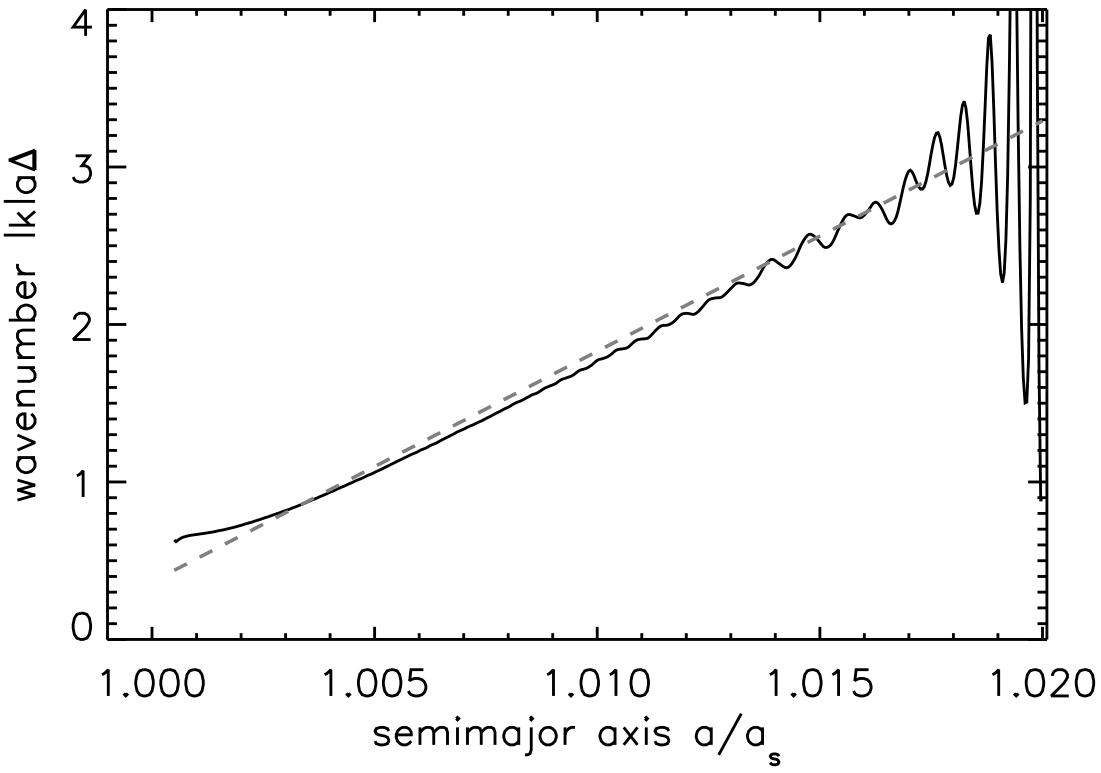
4
3
2
1
0
wavenumber |k|aΔ
1.000
1.005
1.010
1.015
1.020
semimajor axis a/a_s

Fig. 5.— The upper figure shows the disk's longitude of ascending nodes $\Omega(a)$ relative to the satellite's node Ω_s, in units of π, for the simulation of Fig. 4 at time $t = 75 \times 10^3$ orbits, when the wave has swept across the disk. The lower figure shows the dimensionless wavenumber $|k|a\Delta$ at this moment, where wavenumber is calculated from $k = -\partial\Omega/\partial a$. Note that the simulated curve gets a bit ragged at the disk's outer edge, which is where the bending wave is just starting to reflect. The dashed line is the expected wavenumber, Eqn. (46), with $\varepsilon = 1$. This spiral pattern has an initial wavenumber of about $|k_0|a\Delta = 0.63$ at the disk's inner edge.

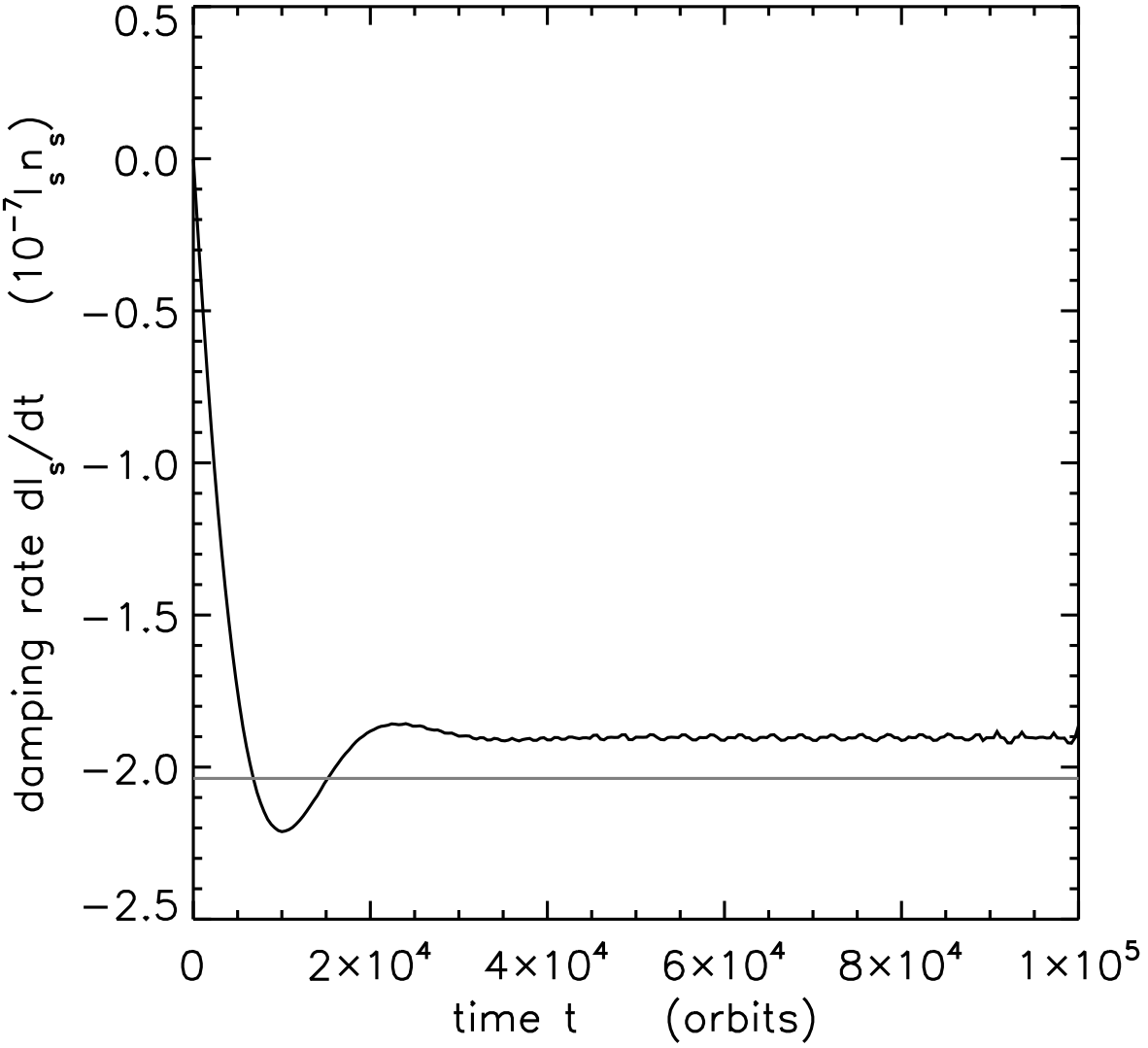

Fig. 6.— The rate at which the satellite launching the wave in Fig. 4 has its inclination damped, $\dot{I}_s$, is plotted versus time t (in units of orbit periods). The solid gray curve is the expected rate, from Eqn. (50) assuming $|k_0|a\Delta = 0.63$ and $C(|k_0|a\Delta) = 0.32$, where C is obtained from Fig. 3.

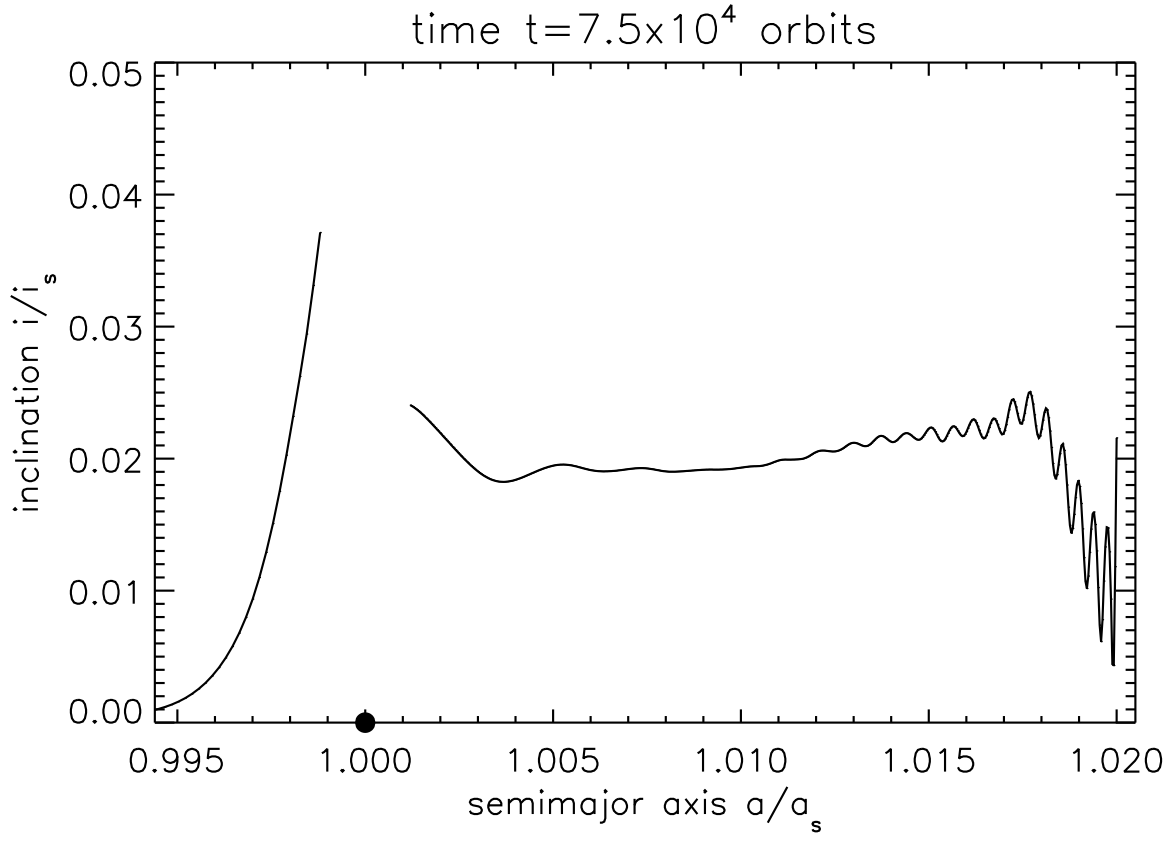
time t=7.5x10^4 orbits
inclination i/i_s
0.05
0.04
0.03
0.02
0.01
0.00
0.995
1.000
1.005
1.010
1.015
1.020
semimajor axis a/a_s

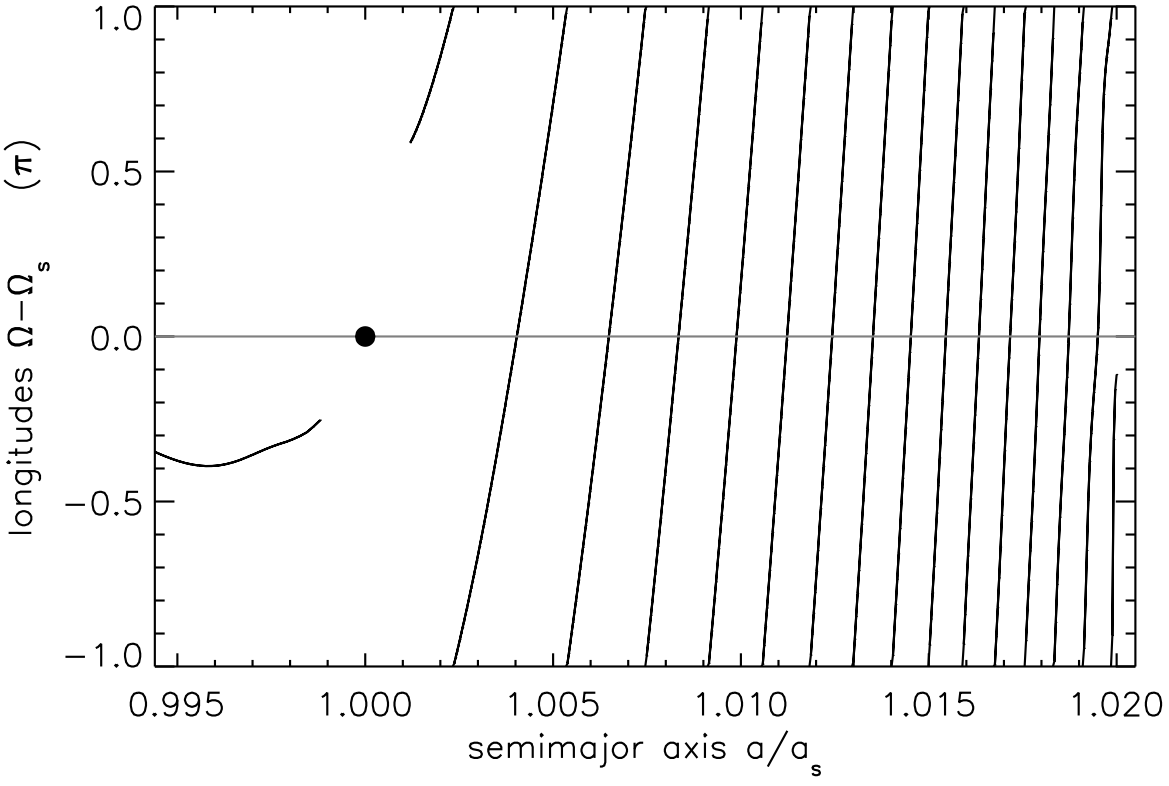
longitudes Ω−Ω_s (π)
1.0
0.5
0.0
−0.5
−1.0
0.995
1.000
1.005
1.010
1.015
1.020
semimajor axis a/a_s

Fig. 7.— A simulation of spiral bending waves launched by an inclined Pan orbiting in the Encke gap in Saturn's A ring. Figures show the disk inclinations $I(a)/I_s$ and relative longitudes $\Omega(a) - \Omega_s$ plotted versus semimajor axis a at time $t = 7.5 \times 10^4$ orbits, which is the time it takes the spiral bending wave to propagate across the simulated 'disk'. Note that the simulated disk is actually quite narrow since it only extends over $0.99 \leq a/a_s \leq 1.02$. The system parameters are: Pan's mass $\mu_s = 8.7 \times 10^{-12}$ (Porco 2005), semimajor axis $a_s = 1.34 \times 10^5$ km, inclination $\sin i_s = 10^{-5}$, with an A ring surface density $\sigma = 50$ gm/cm^2 (Rosen et al. 1991) and a normalized disk mass of $\mu_d = \pi\sigma a_s^2/M_S = 5 \times 10^{-8}$. The gap half–width is $\Delta a_s = 160$ km (Burns et al. 2005), so its fractional half–width is $\Delta = 0.0012$. $N = 500$ rings are used to to simulate the wave in the disk exterior to the satellite, while 50 rings are used to resolve the disturbance in the interior disk. The rings' fractional half–widths $\mathfrak{h}$ are set equal to their separations. Saturn's second zonal harmonic is $J_2 = 0.0163$ and the planet's radius is $R_p = 0.45 a_s$, so the system's critical disk mass, Eqn. (43), is $\mu_c = 7.8 \times 10^{-8}$.

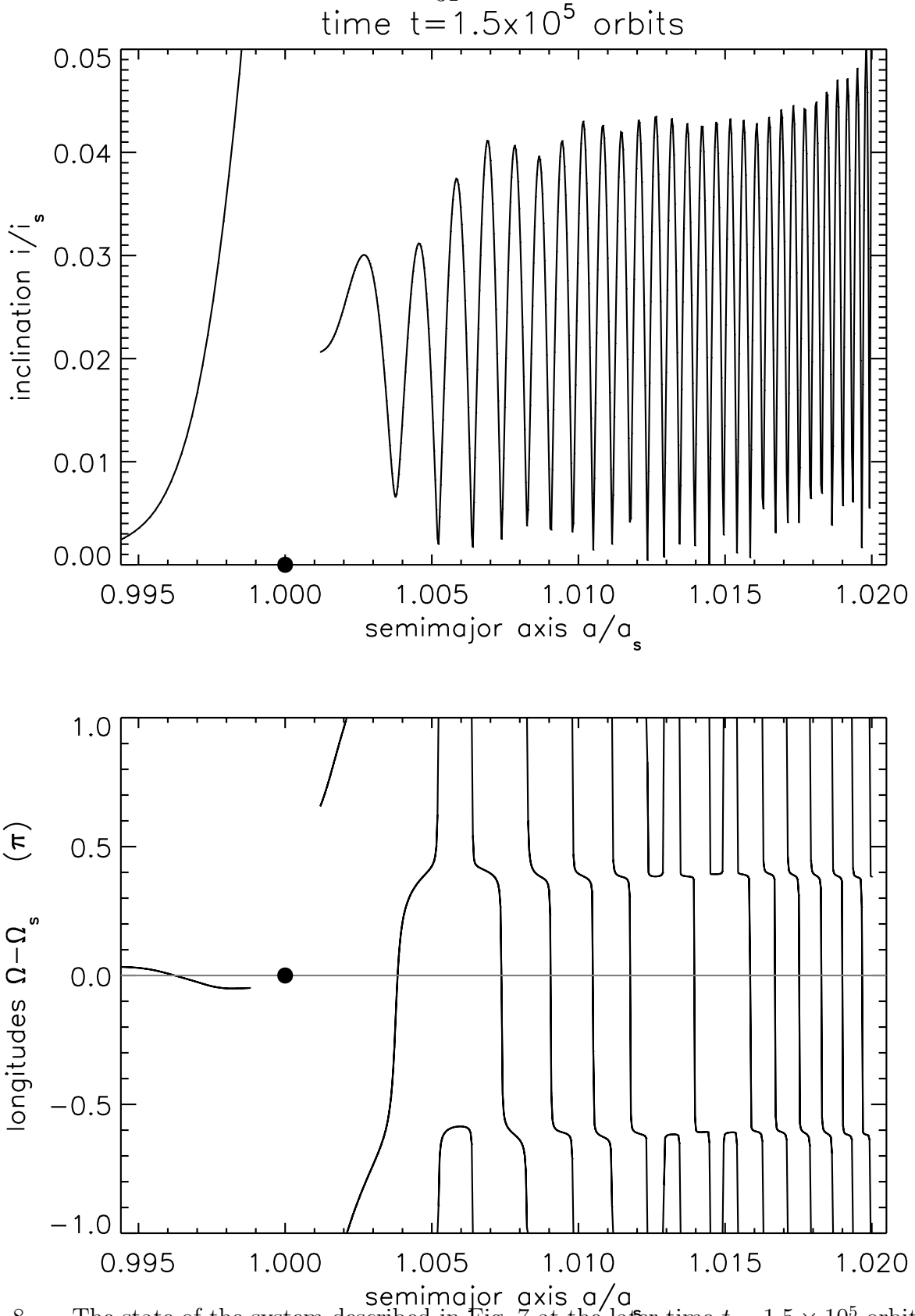

Fig. 8.— The state of the system described in Fig. 7 at the later time $t = 1.5 \times 10^5$ orbits, which is when the bending wave has reflected at the simulated disk's outer edge and returned to the launch site, thereby establishing a standing wave in the disk. The fractional error in this system's total angular momentum is $|\Delta L_i/L_i| < 5 \times 10^{-5}$.